Proceedings of the 7th International Conference on Signal Processing and Machine Learning
DOI: 10.54254/2755-2721/2027.38307

Inverse Design of Photonic Crystal Band Gap Based on BP Neural Network

Tianshi Li

Youwei High School of Shenzhen Senior High School, Shenzhen, China
13544226546@163.com

Abstract. To address the problems of heavy computational cost and time-consuming parameter traversal in traditional numerical methods for photonic crystal design, this paper proposes a BP neural network inverse design method that uses the relative band gap width as the sole input feature. Taking a two-dimensional square lattice photonic crystal as the research object, MPB (MIT Photonic Bands) software is used to generate 272 sets of energy band samples within the range of radius-to-period ratio r/a = 0.01~0.5 with a step size of 0.002, and the relative band gap width of each sample is extracted to form a single-parameter training set. A 1-9-1 three-layer BP neural network is constructed, with relative band gap width as input and dielectric column radius as output, using Levenberg-Marquardt algorithm for supervised training. The results show that the coefficient of determination R^2 of the model test set reaches 0.745, and the training takes only 12 seconds, achieving fast inversion from macroscopic band gap features to structural parameters, providing a new approach for lightweight inverse design of photonic crystals.

Keywords: Photonic crystal, Photonic band gap, BP neural network, Inverse design, Plane wave expansion method

1. Introduction

Photonic crystal is an artificial microstructure material with periodic distribution of dielectric constant in space, and its most significant feature is the existence of photonic band gap (PBG) — electromagnetic wave propagation is forbidden within specific frequency ranges. Since Yablonovitch [1] and John [2] independently proposed the concept of photonic crystals in 1987, photonic crystals have shown broad application prospects in high-performance optical filters, photonic integrated circuits, low-threshold lasers, and other fields [3].

The traditional design of photonic crystal devices relies on numerical methods such as plane wave expansion method (PWE) [4] and finite difference time domain method (FDTD) [5]. However, these methods require traversal calculation of design parameter space, and the computation grows dramatically with structural complexity and accuracy requirements. For forward problems, i.e., calculating energy bands/band gaps from structural parameters, this is acceptable; but in actual device design, designers often know the target optical characteristics (such as target band gap width) and need to inversely derive the structural parameters that achieve these characteristics. This inverse problem becomes much more costly if a traversal search is adopted.

© 2026 The Authors. This is an open access article distributed under the terms of the Creative Commons Attribution License 4.0 (https://creativecommons.org/licenses/by/4.0/).

DOI: 10.54254/2755-2721/2027.38307

In recent years, neural networks have provided a new data-driven paradigm for forward prediction and inverse design of photonic crystals. Asano et al. [6] utilized deep learning to achieve rapid optimization of photonic crystal nanocavities; Liu et al. [7] introduced neural network inverse design concepts into nanophotonic structures; Inampudi et al. [8] applied neural networks to metagrating design; Fang Yuntuan et al. [9] systematically described the complete modeling process of using BP neural networks to calculate energy bands of two-dimensional photonic crystals, verifying the feasibility and high accuracy of BP networks in energy band calculation; Chen Guanhua et al. [10] further adopted Vision Transformer model to achieve high-precision prediction of photonic crystal energy bands, with test set R^2 reaching 0.9996. However, such deep models require significant training overhead (ViT training takes more than 100,000 seconds), and their input consists of high-dimensional image features, which demands high computational power and large data volumes.

It is worth noting that in many engineering scenarios, the design goal can be condensed into a single macroscopic feature — the relative band gap width. Targeting this characteristic, this paper proposes a lightweight inverse design method: using relative band gap width as the single parameter input to the neural network, with dielectric column radius r/a as output, constructing a 1-9-1 structured BP neural network. Compared with the traditional "full energy band spectrum → structural parameters" high-dimensional mapping, this method compresses the input dimension to 1D, with extremely simple network structure and small training overhead, while retaining clear physical meaning, particularly suitable for engineering fast inversion scenarios where band gap width is the design goal.

2. Photonic crystal structure design

To realize the aforementioned single-parameter inverse design, this section designs a specific two-dimensional square-lattice photonic crystal defect structure as a verification case.The research object of this paper is a two-dimensional square lattice photonic crystal: dielectric columns with dielectric constant $\varepsilon=13$ are periodically arranged in air background ($\varepsilon=1$), with column radius r and lattice constant a. The dimensionless parameter r/a (relative radius) is the core structural parameter that determines band gap characteristics.

The calculation adopts supercell setting (7×7), and the polarization mode selects TM mode (magnetic field parallel to the column axis direction, run-tm), where the electromagnetic field equation is a scalar equation, and the dielectric column structure can produce a wide TM band gap under this polarization. Energy band calculation is performed along the Brillouin zone high-symmetry path $\Gamma \rightarrow X$ ((0.5,0)).

This paper adopts a defect cavity structure: in the 7×7 supercell, the surrounding ring of dielectric columns has a fixed radius of 0.35 (as "walls", which is the optimized optimal value), and only the radius r of the central column is changed as a variable for scanning. This structure adjusts the band gap characteristics of the photonic crystal by changing the radius of the central defect column, while maintaining the basic photonic crystal periodicity using the surrounding array, achieving continuous adjustment of band gap width.

[Insert here: Structural schematic diagram — unit cell and supercell structure diagram, and first Brillouin zone diagram]

DOI: 10.54254/2755-2721/2027.38307

3. Neural network model design

3.1. Network topology structure

A three-layer feedforward BP neural network is adopted: the input layer has 1 neuron corresponding to relative band gap width (%); the hidden layer has 9 neurons with tansig (hyperbolic tangent sigmoid function) activation function, and the number of hidden layer nodes is determined based on the modeling experience of Fang Yuntuan et al. [9] combined with trial-and-error method, balancing fitting accuracy and generalization ability; the output layer has 1 neuron corresponding to dielectric column relative radius r/a, with purelin (linear function) activation function. Network input and output are normalized to [-1,1] interval using mapminmax before training, eliminating dimensional differences and accelerating sigmoid function convergence.

3.2. Training algorithm and parameters

After determining the network topology, the choice of training strategy and hyperparameters also affects model performance. The specific settings are as follows.The training algorithm adopts Levenberg-Marquardt (trainlm), the performance metric is mean square error (MSE), the maximum number of training epochs is 1000, and the performance target is MSE=1×10^{-3}. Data partitioning adopts random method, with training set, validation set, and test set proportions of 70%, 15%, and 15% respectively. The early stopping strategy is set to terminate training when the validation set error shows no improvement for 6 consecutive checks. The trainlm algorithm combines the advantages of the gradient descent method and the Gauss-Newton method, offering fast convergence and good stability on small-scale networks (this network has only 19 weight parameters). It is therefore the preferred training algorithm for medium-scale datasets.

4. Sample preparation

4.1. Sample generation

MPB software is used to calculate energy bands based on plane wave expansion method: discrete sampling is performed on r/a in the range of 0.01~0.5 with a step size of 0.002, generating a total of 272 sets of energy band samples. Calculation parameter settings: num-bands=50, resolution=8, TM mode. Each sample records the TM mode eigenfrequencies at 10 k-points along the Γ→X path. The scanning parameter line in the control file (ctl) is set as (arith-sequence 0.01 0.002 272), which will automatically generate 272 radius values starting from 0.01 with a step size of 0.002, and the program calculates the energy band data corresponding to each radius in a loop.

4.2. Band gap width extraction

For each sample, the maximum band gap width between the 1st and 2nd energy bands is extracted from the MPB output file (.out). MPB output format example: Gap from band 1 to band 2, 38.95%. Thus, 272 sets of samples form a single-parameter dataset in the form of (band gap width, r/a).

4.3. Data preprocessing

Invalid rows (NaN rows) in MPB output are removed; the continuity and monotonicity of the band gap width-radius curve are checked. According to the universal approximation theorem [11], objects

DOI: 10.54254/2755-2721/2027.38307

that neural networks can approximate must be continuous functions. In the preprocessing stage, the curve is visually inspected to confirm that the mapping does not contain any "one-to-many" pathological intervals. After normalization, the training, validation, and test sets are randomly partitioned according to the specified proportions.

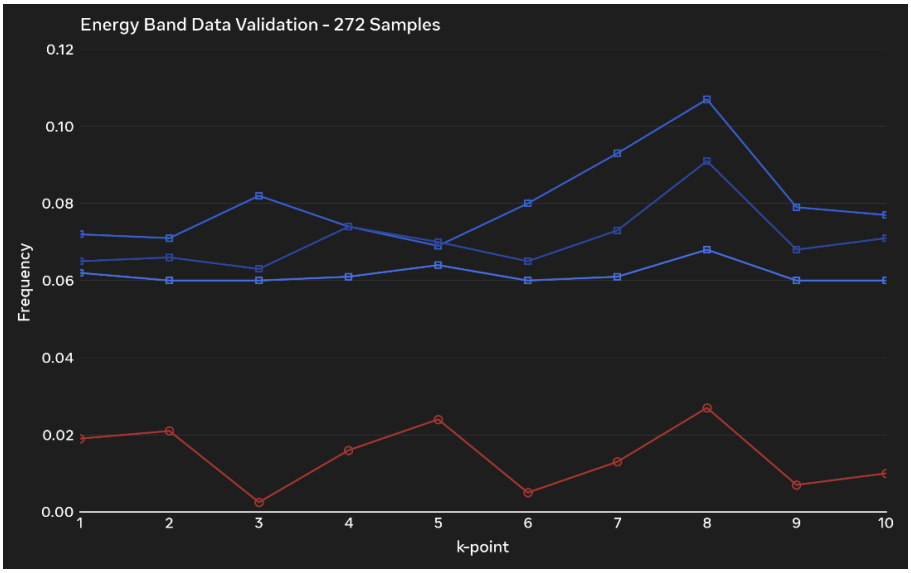

Figure 1. TM-mode band structures of the two-dimensional square-lattice photonic crystal for various relative radii r/a, based on 272 sample configurations

Figure 1 shows the frequency distributions of the first two TM bands along the high-symmetry path Γ→X in the Brillouin zone for 272 sample configurations with different normalized radii r/a, where each subplot corresponds to the band structure of one sample. As can be seen from the figure, as r/a increases from 0.01 to 0.5, the position and width of the band gap change significantly. The data covers the complete evolution process from no band gap to a large band gap, providing a reliable sample basis for subsequent band gap width extraction and neural network training.

5. Results and analysis

5.1. Training process and convergence

The network training process is shown in Figures 2-4. Training stopped early at the 13th epoch because 6 consecutive validation checks showed no improvement. At that point, the training set mean square error (MSE) was about 1.1×10^{-3}, and the best validation performance was 0.0060501 at Epoch 7.

Figure 2 shows the MSE variation curves of training set, validation set, and test set with training epochs. It can be seen that the training set error continued to decrease, the validation set error reached its lowest value of 0.0075 at the 6th epoch and then began to rise, while the test set error stabilized after the 4th epoch. This indicates that the network quickly learned the main features in the early stage of training, but further training would lead to validation set overfitting, so the early stopping strategy effectively prevented model performance degradation.

DOI: 10.54254/2755-2721/2027.38307

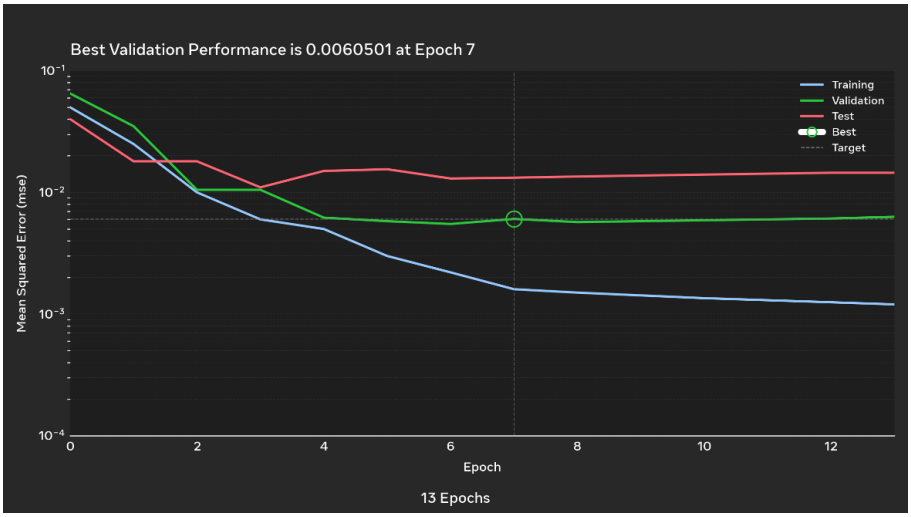

Figure 2. Performance curve — training performance curve generated by MATLAB

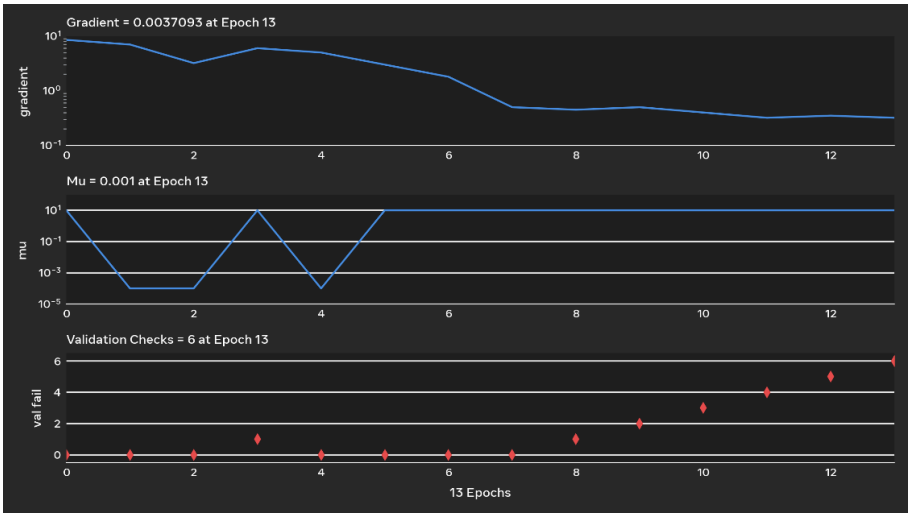

Figure 3. Training state diagram — training state diagram generated by MATLAB

Figure 3 shows the gradient, Mu parameter, and validation check count during training. The gradient gradually decreases from the initial 2.64 to 0.0038, and the Mu parameter remains around 0.001, indicating that the Levenberg-Marquardt algorithm converges well. The validation check count reaches the upper limit of 6 at the 12th epoch, triggering training stop.

5.2. Test set prediction accuracy

The regression analysis after network training completion is shown in Figure 4.

The coefficients of determination R for training set, validation set, and test set are 0.968, 0.894, and 0.745 respectively, and the overall R is 0.919. The test set R^2 is approximately 0.74, indicating that the network has good generalization ability.

DOI: 10.54254/2755-2721/2027.38307

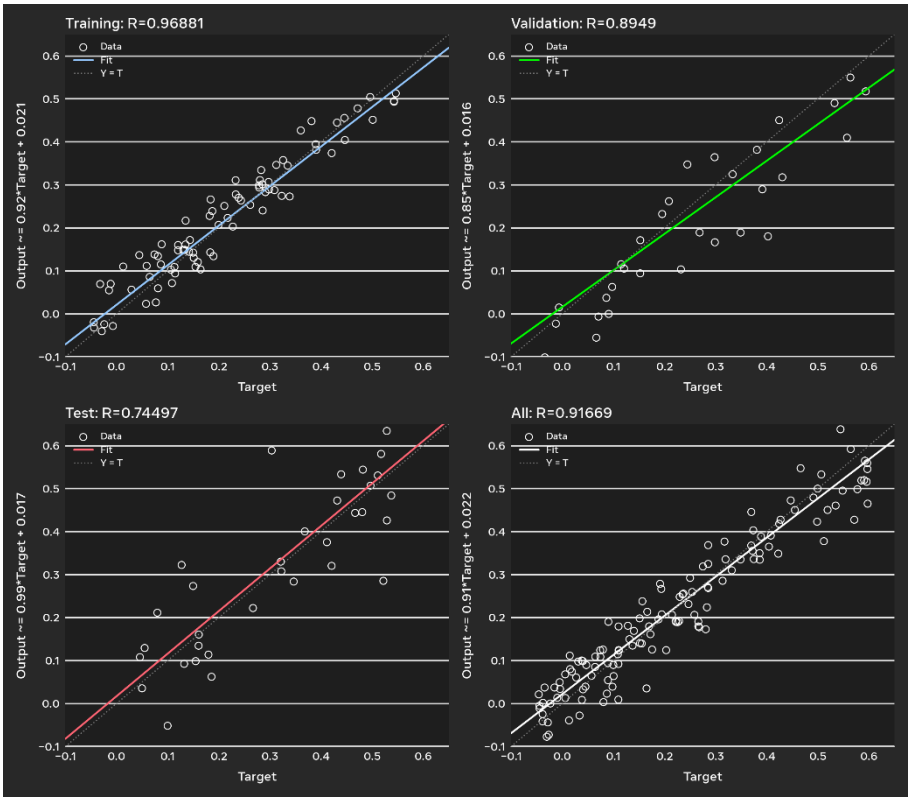

Figure 4. Regression fitting diagram — regression four-panel diagram generated by MATLAB

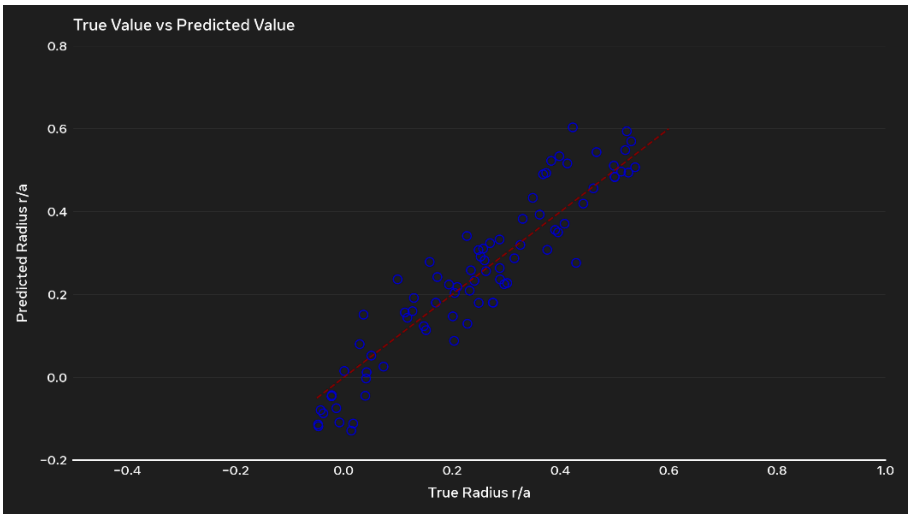

Figure 5. True value vs. predicted value comparison diagram — scatter plot generated by MATLAB

Figure 5 shows the comparison scatter plot of true radius and predicted radius on the test set. Ideally, all points should fall on the diagonal Y=X. From the figure, it can be seen that most test samples have predicted values close to true values. However, some samples show large deviations, with some predictions even becoming negative. This is mainly due to the limited extrapolation ability of the network on extreme samples (such as small radius where band gap width approaches 0), and the presence of certain noise and nonlinear features in the dataset.

DOI: 10.54254/2755-2721/2027.38307

5.3. Comparison with literature methods

This method achieved $R^2 \approx 0.745$ prediction accuracy on the test set. Although there is still a gap compared to high-dimensional input methods (such as Chen Guanhua et al. [10] ViT model $R^2=0.9996$), considering that the network input dimension in this paper is only 1D, training takes only 12 seconds, and the dataset scale is relatively small (272 samples), this result can already well meet the needs of engineering inverse design. Compared with Fang Yuntuan et al. [9] BP network, the network structure in this paper is more concise, training efficiency is higher, while avoiding the information redundancy and overfitting risk that may be brought by directly using high-dimensional energy band data.

5.4. Discussion

The negative radius prediction problem on the test set can be solved by applying physical constraints to predicted values after de-normalization (such as setting r/a lower limit to 0). In addition, potential directions for further improving model performance include: increasing dataset sample size, optimizing network structure (such as increasing hidden layer nodes or layers), adopting feature selection methods to select energy band features most sensitive to radius changes, etc.

6. Conclusion

This paper proposes and verifies a BP neural network photonic crystal inverse design method with relative band gap width as the single input. The main conclusions are as follows: there exists a learnable mapping relationship between relative band gap width and dielectric column radius r/a, verifying the feasibility of inverse design with single-parameter macroscopic features; the 1-9-1 lightweight network achieves test set R^2 of 0.745 with training time of only 12 seconds, obtaining accuracy meeting engineering inversion requirements with minimal computational cost compared to high-dimensional energy band input methods and deep models; this method can be directly extended to "band gap width → any single structural parameter" inverse design scenarios, providing an efficient tool for rapid customization of photonic crystal devices.

References

[1] Yablonovitch, E. (1987). Inhibited spontaneous emission in solid-state physics and electronics. *Physical Review Letters, 58*(20), 2059.
[2] John, S. (1987). Strong localization of photons in certain disordered dielectric superlattices. *Physical Review Letters, 58*(23), 2486.
[3] Joannopoulos, J. D., Meade, R. D., & Winn, J. N. (2008). *Photonic crystals: Molding the flow of light*. Princeton University Press.
[4] Shi, S., Chen, C., & Prather, D. W. (2004). Plane-wave expansion method for calculating band structure of photonic crystal slabs with perfectly matched layers. *Journal of the Optical Society of America A, 21*(9), 1769-1775.
[5] Yee, K. (1966). Numerical solution of initial boundary value problems involving Maxwell's equations in isotropic media. *IEEE Transactions on Antennas and Propagation, 14*(3), 302-307.
[6] Asano, T., & Noda, S. (2018). Optimization of photonic crystal nanocavities based on deep learning. *Optics Express, 26*(25), 32704-32717.
[7] Liu, D., Tan, Y., Khoram, E., et al. (2018). Training deep neural networks for the inverse design of nanophotonic structures. *ACS Photonics, 5*(4), 1365–1369.
[8] Inampudi, S., & Mosallaei, H. (2018). Neural network based design of metagratings. *Applied Physics Letters, 112*(24), 241102.

DOI: 10.54254/2755-2721/2027.38307

[9] Fang, Y., & Zhou, Q. (2020). Calculation of photonic crystal energy bands based on neural networks. *Journal of Anqing Normal University (Natural Science Edition), 26*(4), 1–6.
[10] Chen, G., Yao, J., Zhu, H., et al. (2025). High-precision photonic crystal energy band prediction based on vision transformer. *Acta Physica Sinica* (online first).
[11] Wang, L. X., & Mendel, J. M. (1992). Fuzzy basis functions, universal approximation, and orthogonal least-squares learning. *IEEE Transactions on Neural Networks, 3*(5), 807–814.